The mesolayer of attached eddies in wall-bounded turbulent flows

Yongyun Hwang

Department of Aeronautics
Imperial College London
South Kensington, SW7 2AZ, London, UK
y.hwang@imperial.ac.uk

ABSTRACT

It has recently been reported that the outer peak in the second-order statistics of the streamwise velocity depends on the Reynolds number. Starting from this puzzling observation, here I propose that the streamwise velocity component of each of the energy-containing motions in the form of Towsnend's attached eddies exhibit inner-scaling nature in the region close to the wall (see figure 1). Some compelling evidence on this proposition has been presented with a careful inspection of scaling of velocity spectra from direct numerical simulations and a linear analysis with an eddy viscosity. It is shown that this behavior can emerge due to inhomogeneous turbulent dissipation in the wall-normal direction, and also enables one to explain the Reynolds-number-dependent behavior of the outer peak as well as the near-wall penetration of the large-scale outer structures in a consistent manner. Extension of this concept to Townsend's attached eddy hypothesis further reveals that the self-similarity in the streamwise velocity of the attached eddies would be theoretically broken in the region close to the wall.

INTRODUCTION

It has recently been reported that the wall-normal location of the outer peak exhibit dependence on the friction Reynolds number Re_τ: the wall-normal peak location y_{peak} in turbulent boundary layer and pipe flow was shown to be $y^+_{peak} \sim {Re_\tau}^{1/2}$ at least for $Re_\tau \lesssim 20000$, and even the streamwise wavenumber retaining the peak was found depend upon the Reynolds number (Mathis *et al.*, 2009; Vallikivi *et al.*, 2015). This observation is reminiscent of the concept of 'mesolayer' defined for the construction of the mean velocity (Long & Chen, 1981; Afzal, 1982, 1984; Sreenivasan & Sahay, 1997; Wei *et al.*, 2005). The introduction of the mesolayer originates from the observation that the inner-scaled peak wall-normal location of the Reynolds shear stress scales as ${Re_\tau}^{1/2}$ (Long & Chen, 1981), and the related mean momentum balance implies that the viscous wall effect on the mean velocity would not be negligible at least below the peak wall-normal location of the Reynolds shear stress (Sreenivasan & Sahay, 1997; Wei *et al.*, 2005). Given the fact that the outer peak in the spectra of the streamwise velocity would probably indicate very-large-scale motion (VLSM; the long streaky motion in the outer region), the emergence of its Reynolds-number-dependent behavior indicates that this structure, especially the part below the outer peak, would experience some viscous influence of the wall. In this respect, it is interesting to note the recent observations on the influence of the large-scale outer structure to the near-wall motions (Hutchins & Marusic, 2007; Mathis *et al.*, 2009; Agostini & Leschziner, 2014, 2016). The existence of such an inner-outer interaction in the near-wall region would require the large-scale outer structure to reach the near-wall region at least to some extent (i.e. the footprint of the large-scale structure). This indicates that the outer structure in the outer coordinate should extend more to the wall on increasing the Reynolds number, resulting in a feature which would be difficult to explain if the large-scale structure scales only in the outer length scale.

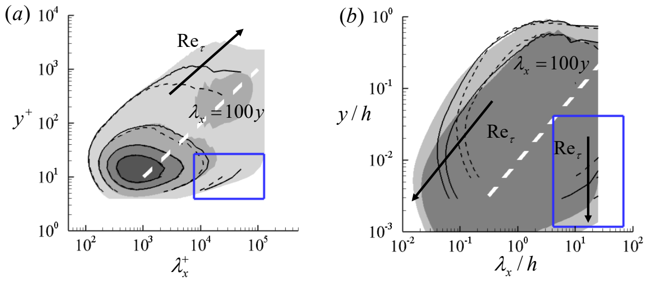

Figure 1. Premultiplied streamwise wavenumber spectra of streamwise velocity (a) in the $\lambda_x^+ - y^+$ plane and (b) in the $\lambda_x/h - y/h$ plane. The contour labels in (a) are 0.2, 0.4, 0.6, and 0.8 times of each maximum, while those in (b) are 0.1 and 0.2 times of each maximum. Here, the dashed, solid and shaded contours are respectively from $Re_\tau = 934$, $Re_\tau = 2003$ (Hoyas & Jiménez, 2006) and $Re_\tau = 5186$ (Lee & Moser, 2015). In each case, the region of interest is highlighted with a box.

The speculated feature is shown in Fig. 1 where the streamwise wavenumber spectra of streamwise velocity of turbulent channel flow are given from direct numerical simulation data available at $Re_\tau = 934, 2003, 5186$ (Hoyas & Jiménez, 2006; Lee & Moser, 2015) where $Re_\tau = u_\tau h/\nu$ (u_τ is the friction velocity, ν kinematic viscosity, and h half-height of the channel). Not surprisingly, if the spectra are scaled by the inner unit, they all show very good agreement in the near-wall region (figure 1a; here λ_x is the streamwise wavelength). As the Reynolds number increases, the energetic part of the spectra exhibits a linear growth with y along the ridge $\lambda_x \simeq 100y$ (y is the wall-normal distance from the wall), indicating the emergence of a large number of self-similar streaky motions in the logarithmic region found in Hwang (2015). However, even in the near-wall region, it is important to note that the good inner scaling of the spectra appears only for $\lambda_x^+ \lesssim O(10^3)$: the spectra for $\lambda_x^+ \gtrsim O(10^4)$ in the region of $y^+ \lesssim 50$ become increasingly more energetic and longer on increasing the Reynolds number (the blue-boxed region in figure 1a), indicating the growing near-wall influence of the energy-containing flow structures in the logarithmic and outer regions at higher Reynolds numbers. This feature is also confirmed in the outer-scaled spectra (figure 1b). The outer-scaled spectra appear to scale very well in the outer unit for $\lambda_x > 1h$ and $y > 0.2 \sim 0.3h$, the region directly related to large-scale motions (LSMs) and VLSMs. While the spectra extend to the wall mainly along $\lambda_x \simeq 100y$ on increasing the Reynolds number, the part of the spectra at $\lambda_x \simeq 10 \sim 20h$ also appears to extend to the wall with the increase of the Reynolds number (the blue-boxed region in figure 1b), confirming that the near-wall part (i.e. footprint) of the large-scale outer structure does not scale in the outer unit and that it extends more to the wall on increasing the Reynolds number.

Given the wall-normal location of the near-wall part of the

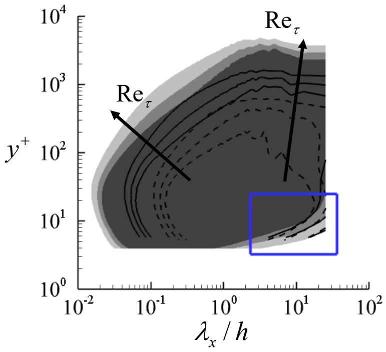

Figure 2. Premultiplied streamwise wavenumber spectra of the streamwise velocity in $\lambda_x/h - y^+$ plane. The labels of each contour are given to be uniformly spaced from zero for comparison of the wall-normal structure of the spectra in the region highlighted with the blue box. Here, the dashed, solid and shaded contours are respectively from $Re_\tau = 934$, $Re_\tau = 2003$ (Hoyas & Jiménez, 2006) and $Re_\tau = 5186$ (Lee & Moser, 2015).

large-scale outer structure, the only relevant length scale for it to be properly scaled would be the inner length scale. We therefore replot the spectra given in Fig. 1 in the $\lambda_x/h - y^+$ plane in figure 2. If each of the spectra at three different Reynolds numbers is properly normalized, the wall-normal structure of the streamwise velocity spectra at $\lambda_x \simeq 10 \sim 20h$ exhibits good scaling with the inner unit in the near-wall region (the blue-boxed region in figure 2), indicating the near-wall part of the large-scale outer structures is affected by viscous effect of the wall. It is important to mention that, from the scaling viewpoint, this observation indicates that the wall-normal location of the outer peak should be an outcome of an asymptotic matching between two functions, one of which scales in the inner unit in the near-wall region (fig 2) and the other scales in the outer unit in the outer region (fig 1*b*), resulting in the Reynolds-number-dependent behavior of the outer peak.

This intriguing feature of the large-scale outer structure evidently reminds us of the concept of 'mesolayer' originally introduced for mean-momentum balance (e.g. Wei *et al.*, 2005). It also leads us to several important related questions: What is the origin of the inner-scaling nature of the large-scale outer structure?; Is it also observed in the self-similar energy-containing motions in the logarithmic region (Townsend, 1976; Perry & Chong, 1982; Hwang, 2015)? What is its consequence to the classical theory on the coherent structures (Townsend, 1976)? To answer these questions, here we carefully reinspect the linear theory used in our previous studies (Cossu *et al.*, 2009; Pujals *et al.*, 2009; Hwang & Cossu, 2010*a*,*b*; Willis *et al.*, 2010), where optimal transient growth of small organised perturbations is calculated using the linearized Navier-Stokes equation with an appropriate eddy viscosity (Reynolds & Hussain, 1972). We subsequently show that the most amplified mode in the linear theory exhibits the qualitatively same behavior with the spectra of DNS (figures 1 and 2). Generalization of this observation is then made to the modes emerging in the form of Townsend's attached eddies (Hwang & Cossu, 2010*b*), revealing that the presence of such an inner-scaling region of each attached eddy should lead to theoretically 'broken' self-similarity of the log-layer motions in the region close to the wall. The origin of this behavior is then studied by carefully examining the linearized Navier-Stokes equation, and we will see that this feature is essentially due to inhomogeneous turbulent dissipation in the wall-normal direction.

LINEAR MODEL

Equation for a small-amplitude motion of interest

We consider a fluid flow over a turbulent channel in which the streamwise, wall-normal and spanwise directions are denoted by x, y, and z, respectively. The two walls are set to be located at $y = 0$ and $y = 2h$, respectively. Density and kinematic viscosity of the fluid are denoted by ρ and ν. The velocity field in the channel is denoted by $\mathbf{u} = (u, v, w)$ where u, v and w indicate the streamwise, wall-normal and spanwise velocities, respectively. Following Reynolds & Hussain (1972), the velocity field $\mathbf{u}$ may be decomposed into

$$\mathbf{u} = \mathbf{U} + \mathbf{u}' + \tilde{\mathbf{u}}, \tag{1}$$

where $\mathbf{U} = (U(y), 0, 0)$ is the mean velocity, $\mathbf{u}'$ turbulent velocity fluctuation, and $\tilde{\mathbf{u}}$ is the 'organized wave' of interest. If the amplitude of $\tilde{\mathbf{u}}$ is 'small' and an appropriate closure is provided for describing the role of $\mathbf{u}'$ in evolution of $\tilde{\mathbf{u}}$, the equation for $\tilde{\mathbf{u}}$ is given by

$$\nabla \cdot \tilde{\mathbf{u}} = 0, \tag{2a}$$

$$\frac{\partial \tilde{\mathbf{u}}}{\partial t} + (\tilde{\mathbf{u}} \cdot \nabla)\mathbf{U} + (\mathbf{U} \cdot \nabla)\tilde{\mathbf{u}} = -\frac{1}{\rho}\nabla \tilde{p} + \nabla \cdot \left[(\nu + \nu_t) \left(\nabla \tilde{\mathbf{u}} + \nabla \tilde{\mathbf{u}}^T \right) \right], \tag{2b}$$

with the initial condition

$$\tilde{\mathbf{u}}(x, y, z, t = 0) = \tilde{\mathbf{u}}_0(x, y, z). \tag{2c}$$

Here, $\tilde{p}$ is the related pressure and ν_t is the eddy viscosity, for which the semi-empirical expression by Cess (1958) is adopted (e.g. Butler & Farrell, 1993; del Álamo & Jiménez, 2006; Pujals *et al.*, 2009; Hwang & Cossu, 2010*b*):

$$\begin{aligned} \nu_t(\eta) = \; & \frac{\nu}{2}\Big\{1 + \frac{\kappa^2 Re_\tau^2}{9}(1-\eta^2)^2(1+2\eta^2)^2 \times \\ & \{1 - \exp[(|\eta| - 1)Re_\tau/A]\}^2\Big\}^{1/2} - \frac{\nu}{2}, \end{aligned} \tag{3}$$

where $\eta = (y-1)/h$, $\kappa = 0.426$ and $A = 25.4$ from del Álamo & Jiménez (2006). We note that the eddy viscosity has a direct relation with the mean velocity profile $U(y)$ through the mixing length model: i.e. $\nu_t dU/dy = -\overline{u'v'}$.

Optimal transient growth

Now, we consider a plane Fourier mode, such that: $\tilde{\mathbf{u}}(x, y, z, t) = \hat{\mathbf{u}}(y, t)e^{i(\alpha x + \beta z)}$, where α and β are the streamwise and spanwise wavenumbers, respectively (i.e. $\alpha = 2\pi/\lambda_x$ and $\beta = 2\pi/\lambda_z$). Since the linearized system for each Fourier mode been found to be stable in all the canonical wall-bounded shear flows considered so far (Cossu *et al.*, 2009; Pujals *et al.*, 2009; Hwang & Cossu, 2010*a*,*b*; Willis *et al.*, 2010), the amplification mechanism by $\mathbf{A}$ is examined by calculating the so-called optimal transient growth of initial condition. For a given set of α and β, the related optimization problem for initial condition is defined by

$$G_{\max} = \max_t \max_{\hat{\mathbf{u}}_0} \frac{\|\hat{\mathbf{u}}(t)\|^2}{\|\hat{\mathbf{u}}_0\|^2}. \tag{4}$$

The optimization problem is solved using the standard method given e.g. in Schmid & Henningson (2001). The discretization in the wall-normal direction is performed using a Chebyshev collocation method (Weideman & Reddy, 2000) with up to $N_y = 1024$ to manage the highest Reynolds number considered here ($Re_\tau = 40000$). Since an extensive discussion on $G_{\max}$ was made in Pujals *et al.* (2009) and Hwang & Cossu (2010*b*), the focus on the present study will be given to the wall-normal structure of $\hat{\mathbf{u}}_{opt}$ at $t = t_{max}$, which represents the most amplified flow structure by (2), in relation to its similarity to the observation made with the spectra (figures 1 and 2).

Relevance and limitations

Before exploiting the result from the present linear approach, here we address the physical relevance and limitations of the present approach. The linear theory in the present study has been found to be useful for prediction of the generation of the long streaky structures emerging in the near-wall, logarithmic and outer regions (Cossu *et al.*, 2009; Pujals *et al.*, 2009; Hwang & Cossu, 2010*a*,*b*; Willis *et al.*, 2010). Large amplification of $\hat{\mathbf{u}}$ appears typically for $\alpha \ll \beta$, and the resulting velocity field $\hat{\mathbf{u}}_{opt}$ is dominated by a streaky motion of the streamwise velocity. However, the linear theory does not appear to be fully relevant if the wall-normal and spanwise velocities are concerned. In real flow, the main flow structures of these velocity components are typically much shorter than the long streaky structure of the streamwise velocity: the streamwise extent of the flow structure with the intense cross-streamwise velocity fluctuations is only two or three times larger than its spanwise width ($\lambda_x \simeq 2 \sim 3\lambda_z$), whereas the streaky structure of the streamwise velocity appears with ten times larger than that ($\lambda_x \simeq 10\lambda_z$) (Hwang & Cossu, 2010*c*; Hwang, 2015). Given the fact that the linear amplification is large only for $\alpha \ll \beta$, it is questionable whether the linear theory would be fully relevant for such a short wall-normal and spanwise velocity structure. Indeed, it has recently been shown that the length scale of the cross-streamwise velocity components is rather well predicted by instability of the amplified streaky structure, which incorporates some roles of the neglected nonlinearity (Schoppa & Hussain, 2002; Park *et al.*, 2011; Alizard, 2015). A recent numerical experiment further confirmed this by showing that the artificial suppression of the instability of the amplified streak significantly inhibits the generation of the flow structure with the cross-streamwise velocity components (Hwang & Bengana, 2016). Due to this inherent limitation of the present linear approach for description of the wall-normal and spanwise velocities, the primary focus of this paper will be given to the streamwise velocity associated with the linearly amplified long streak.

RESULTS AND DISCUSSION

Now, consider the spanwise wavelength λ_z between $\lambda_z^+ = 100$ and $\lambda_z = 1.5h$. For each λ_z, the streamwise extent of the streaky motions is chosen as

$$\lambda_x \simeq 10\lambda_z, \qquad (5)$$

from Hwang (2015) where the streaky structures in the logarithmic region appear with the scaling given by (5). We note that, if $\lambda_z^+ = 100$, (5) yields $\lambda_x^+ = 1000$, the streamwise length scale of the well-known near-wall streaks. On the other hand, if $\lambda_z = 1.5h$, it gives $\lambda_x = 15h$, the streamwise length scale of the VLSM (the outer streaky structure). At each of the intermediate spanwise length scales λ_z between $\lambda_z^+ = 100$ and $\lambda_z = 1.5h$, (5) gives the streamwise length scale of the self-similar streaky motions in the logarithmic region. For a further discussion on (5), the reader may refer to Hwang (2015).

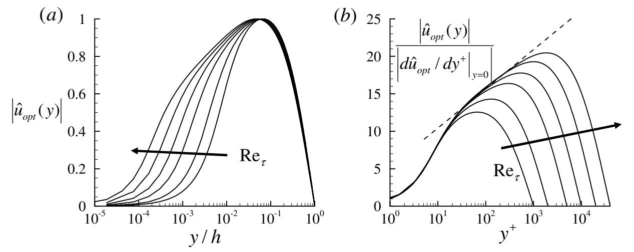

Figure 3. The wall-normal profile of the normalized streamwise velocity of $\hat{\mathbf{u}}_{opt}$ ($\lambda_x = 15h$ and $\lambda_z = 1.5h$): (a) $|\hat{u}_{opt}(y/h)|$; (b) $|\hat{u}_{opt}(y^+)|/|[d\hat{u}_{opt}/dy^+]_{y=0}|$. Here, $Re_\tau = 1000, 2000, 5000, 10000, 20000, 40000$. The dashed line indicates $|\hat{u}_{opt}(y^+)| = 1/0.44\ln(y^+) + 5.2$.

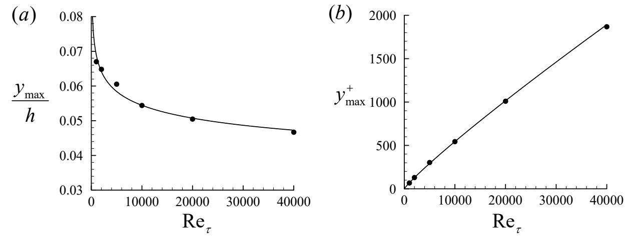

Figure 4. Wall-normal peak location of the streamwise velocity of the optimal response at $t = t_{max}$ with respect to Re_τ. Here, the solid lines in (a) and (b) respectively indicate $y/h = cRe_\tau^{-0.1019}$ and $y^+ = cRe_\tau^{0.8981}$ where c is a fitting constant.

Largest attached eddy: very-large-scale motion

We consider $\lambda_z = 1.5h$ and $\lambda_x = 15h$ from (5), which would represent the VLSM (the outer streaky structure) (Hwang & Cossu, 2010*c*; Hwang, 2015). Fig. 3 shows the normalized $\hat{u}_{opt}(y)$ at $Re_\tau = 1000, 2000, 5000, 10000, 20000, 40000$. If the $\hat{u}_{opt}(y)$ are plotted in the outer coordinate (figure 3*a*), they reveal good accordance to one another in the outer region ($y/h \gtrsim 0.2 \sim 0.3$). In the region close to the wall ($y/h \lesssim 10^{-2}$), such an agreement does not appear: the normalized $\hat{u}_{opt}$ rather gradually extends to the wall on increasing the Reynolds number, similarly to the spectra at $\lambda_x \simeq 10 \sim 20h$ (figure 1*a*). Now, we plot $\hat{u}_{opt}(y)$ in the inner coordinate after normalizing them with the shear rate at the wall, i.e. $d\hat{u}_{opt}/dy^+|_{y=0}$ (figure 3*b*). The rescaled $\hat{u}_{opt}(y)$ show very good scaling in the inner coordinate and can reach the logarithmic region at very high Reynolds numbers, consistent with the spectra in figure 2. Fig. 3 now clearly suggests that $\hat{u}_{opt}(y)$ is a function of only y/h in the outer region (fig 3*a*), while $\hat{u}_{opt}(y)/(d\hat{u}_{opt}/dy^+|_{y=0})$ is a function of only y^+ in the near-wall region (fig 3*b*). It is evident that this feature would lead the peak location of $\hat{u}_{opt}(y)$ (denoted by y_{max}) to be placed in the overlap region with a scaling behavior involving both inner and outer length scales. Such a scaling nature of $\hat{u}_{opt}(y)$ is clearly an analogue to the construction of the mean velocity (e.g. Millikan, 1938; Tennekes & Lumley, 1967), and, interestingly, the logarithmic behavior also appears to emerge in $\hat{u}_{opt}(y)$ for the same reason.

Fig. 4 reports the peak location y_{max} of $\hat{u}_{opt}(y)$ with the Reynolds number. As expected from Fig. 3, the peak location y_{max} reveals the Reynolds-number-dependent behavior, and the best fit of the dependence of y_{max} on Re_τ is found as $y/h \sim Re_\tau^{-0.1019}$. The scaling of y_{max} is not very close to $y/h \sim Re_\tau^{-0.5}$ observed in boundary layer and pipe flows (Mathis *et al.*, 2009; Vallikivi *et al.*, 2015), but this is not so surprising given the number of approximations

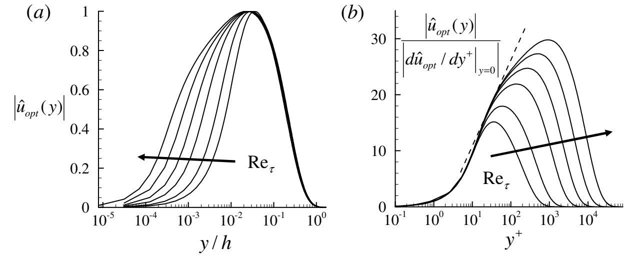

Figure 5. The wall-normal profile of the normalized streamwise velocity of $\mathbf{\hat{u}}_{opt}$ ($\lambda_x = 6h$ and $\lambda_z = 0.6h$): (a) $|\hat{u}_{opt}(y/h)|$; (b) $|\hat{u}_{opt}(y^+)|/|[d\hat{u}_{opt}/dy^+]_{y=0}|$. Here, $Re_\tau = 1000, 2000, 5000, 10000, 20000, 40000$. The dashed line indicates $|\hat{u}_{opt}(y^+)| = 1/0.15\ln(y^+) - 4.5$.

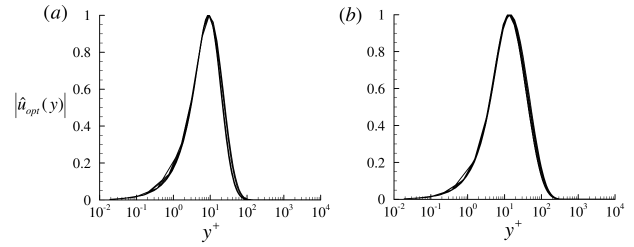

Figure 6. Normalized streamwise velocity profile of the optimal response at $t = t_{max}$: (a) $\lambda_x^+ = 1000$ and $\lambda_z^+ = 100$; (b) $\lambda_x^+ = 3000$ and $\lambda_z^+ = 300$. Here, $Re_\tau = 1000, 2000, 5000, 10000, 20000, 40000$.

made for the present approach (e.g. linearisation, highly simplified eddy viscosity, not fully physical initial condition, etc). However, it is important to note that the dependence of y_{max} on Re_τ appears to be qualitatively the same with the experimental observations, and this is quite encouraging as it is an outcome of the inner-scaling nature observed in Fig. 3 (a).

Attached eddies in the logarithmic region

We now extend the present investigation to the logarithmic region by considering λ_z between $\lambda_z^+ = 100$ and $\lambda_z = 1.5h$, as a spanwise length scale in this range would describe each of the self-similar streaky structures in the logarithmic region (Hwang, 2015; Hwang & Bengana, 2016). We first choose λ_z to scale in the outer unit. Fig. 5 shows the wall-normal profiles of $\hat{u}_{opt}(y)$ at $\lambda_z = 0.6h$ with $\lambda_x = 6h$ for $Re_\tau = 1000, 2000, 5000, 10000, 20000, 40000$. Exactly the same behavior is observed as in Fig. 3. When plotted in the outer coordinate, the normalized $\hat{u}_{opt}(y)$ at the different Reynolds numbers agree well with one another relatively in the outer region (figure 5a). On the other hand, when plotted in the inner coordinate, they collapse well into a single curve in the region relatively close to the wall (figure 5b). The logarithmic dependence of $\hat{u}_{opt}(y)$ is also seen, although the wall-normal size of the related region is much smaller than that with $\lambda_z = 1.5h$ (figure 3) due to the smaller $\lambda_z (= 0.6h)$.

Now, we choose λ_z to scale in the inner unit with the Reynolds number. In this case, the scaling behavior of $\hat{u}_{opt}(y)$ becomes very different from that in figures 3 and 5. Fig. 6 shows the normalized $\hat{u}_{opt}(y)$ in the inner coordinate for $\lambda_z^+ = 100$ and $\lambda_z^+ = 300$ at all the Reynolds numbers considered. In this case, all the profiles of $\hat{u}_{opt}(y)$ are almost identical in the inner coordinate. This suggests that the scaling of the outer part of $\hat{u}_{opt}(y)$ follows the choice of the scaling of λ_z (i.e. the size of the structure of interest). However,

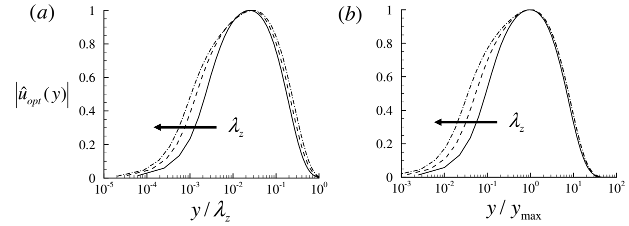

Figure 7. Normalized streamwise velocity profile of the optimal response at $t = t_{max}$ ($Re_\tau = 10000$) in (a) the y/λ_z and (b) y/y_{max} coordinate. Here, $\lambda_z/h = 0.3, 0.6, 0.9$.

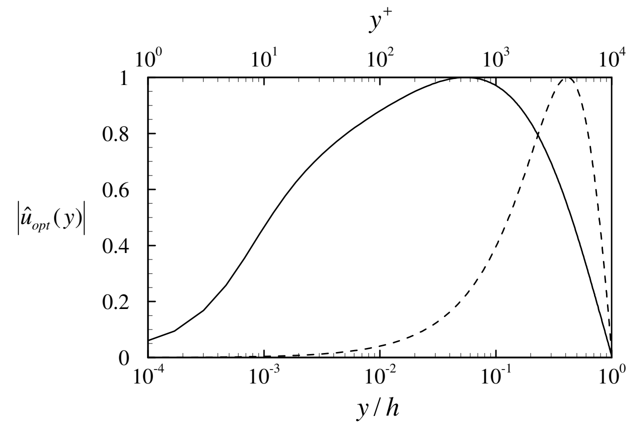

Figure 8. Effect of the eddy viscosity on the normalized streamwise velocity profile of the optimal response at $t = t_{max}$ ($\lambda_z = 1.5h$, $\lambda_x = 15h$, and $Re_\tau = 10000$): (a) the original eddy viscosity; (b) a constant eddy viscosity with $\nu_t = \max_y \nu_t(y)$ where $\nu_t(y)$ is given in (3).

the inner part of $\hat{u}_{opt}(y)$ always remain to scale in the inner unit, no matter how λ_z is chosen.

In our previous study (Hwang & Cossu, 2010b), it was shown that $\hat{u}_{opt}(y)$ for a given λ_z between $\lambda_z^+ = 100$ and $\lambda_z = 1.5h$ is approximately self-similar with respect to λ_z (or y_{max}) as in the attached eddy hypothesis of Townsend (1976). However, more careful observation of $\hat{u}_{opt}(y)$ with figures 5 and 6 now clearly shows that the self-similar nature of $\hat{u}_{opt}(y)$ is valid only in the approximate sense, as the inner part of $\hat{u}_{opt}(y)$ does not appear to be affected by the chosen λ_z. In Fig. 7 (a), $\hat{u}_{opt}$ for $\lambda_z/h = 0.3, 0.6, 0.9$ at $Re_\tau = 10000$ are in the y/λ_z coordinate, and only the outer part of $\hat{u}_{opt}$ seems to be self-similar with respect to λ_z in this coordinate. Scaling with the y/y_{max} coordinate (from $\lambda_z \sim y$), shown in Fig. 7 (b), more precisely confirms that only the outer part of $\hat{u}_{opt}$ scales with $y_{max}(\sim \lambda_z)$, and the near-wall part of $\hat{u}_{opt}(y)$ does not show such a self-similarity. Instead, as λ_z is increased, $\hat{u}_{opt}$ extends more to the wall, indicating that $\hat{u}_{opt}(y)$ would experience incomplete self-similarity due to the inner-scaling nature.

The origin of the inner-scaling nature

The observations of $\hat{u}_{opt}(y)$ so far appear to be consistent with the spectra in figs 1 and 2, so the naturally following question is what would be the origin of this behavior. A careful examination of the linear model reveals that the origin of the inner-scaling nature of $\hat{u}_{opt}(y)$ at least in this case is the eddy viscosity ν_t in (3). Indeed, as shown in Fig. 8, setting the eddy viscosity ν to be constant by $\nu_t = \max_y \nu_t(y)$ inhibits the highly penetrating behavior to the near-wall

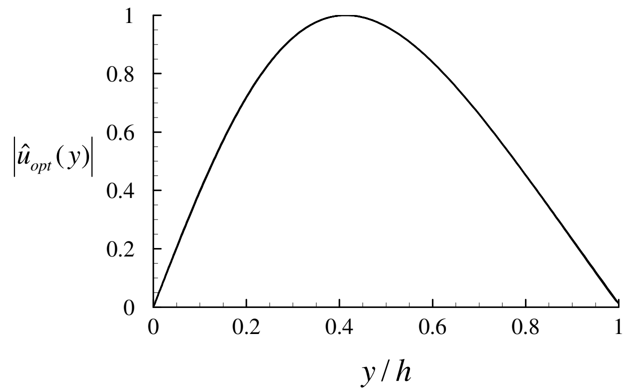

Figure 9. Dependence on the normalized streamwise velocity profile of the optimal response at $t = t_{max}$ on the Reynolds number with a constant eddy viscosity $\nu_t = \max_y \nu_t(y)$. Here, $Re_\tau = 1000, 2000, 5000, 10000, 20000, 40000$. Note that all the profiles considered are almost identical.

region in $\hat{u}_{opt}(y)$ with the original ν_t. In particular, the peak wall-normal location y_{max} of $\hat{u}_{opt}(y)$ is changed from the logarithmic region ($y_{max}/h = 0.055$) to the outer region ($y_{max} = 0.4h$). More importantly, the constant ν_t does not allow $\hat{u}_{opt}(y)$ to depend on the Reynolds number, as shown in Fig. 9. This suggests that the spatially varying original $\nu_t(y)$ in (3) plays a critical role in the large amplification of $\hat{u}_{opt}(y)$ in the near-wall and logarithmic regions as well as the enforcement of the inner-scaling nature of $\hat{u}_{opt}(y)$ in the region close to the wall.

In this respect, it is interesting to take a look at the key feature of ν_t in (3), which originate from its definition given by the mixing length model: i.e.

$$\nu_t \frac{dU}{dy} = -\overline{u'v'}. \qquad (6)$$

In the logarithmic region, the Reynolds stress is constant and $dU/dy \sim 1/y$, thus the considered ν_t should grow linearly with y. What is important here is that this growing behavior of ν_t in the logarithmic region must be generic in any turbulence models for wall-bounded shear flows. In the near-wall region, both of the integral and dissipation length scales are δ_ν, indicating that the dissipation mechanism is dominated by molecular viscosity due to the wall. On the other hand, in the outer region, the integral length scale (h) and the dissipation length scale ($\nu^3 h/u_\tau^3$) are separated with the extent measured by their ratio given by $Re_\tau^{3/4}$. Therefore, in the outer region, a vigorous turbulent dissipation through the energy cascade is expected, resulting in large ν_t from the modelling viewpoint. The only way to incorporate to manage the large disparity between the dissipation mechanisms of the near-wall and outer regions would be by having a smoothly growing ν_t with y, as in (6).

It is important to note that this feature of ν_t plays a critical role in determining the wall-normal structure of $\hat{u}_{opt}(y)$ in the linear theory. In the near-wall region and relatively lower part of the logarithmic region, the given perturbation at $t = 0$ would experience relatively small ν_t, yielding relatively large $\hat{u}_{opt}(y)$ at $t = t_{max}$, whereas in the relatively upper part of the logarithmic region and outer region, it would go through large ν_t, resulting in relatively small $\hat{u}_{opt}(y)$. This simple mechanism explains why $\hat{u}_{opt}(y)$ with ν_t in (3) is larger than that with the constant $\nu_t (= \max_y \nu_t(y))$ in the region close to the wall, while being smaller in the region far from the wall. It is also presumable that such a nature of ν_t in (3) intricately linked to the inner-scaling behavior of $\hat{u}_{opt}(y)$ as demonstrated in Fig. 9. The crucial role of ν_t in the wall-normal structure of $\hat{u}_{opt}(y)$ suggests that the inner-scaling nature of $\hat{u}_{opt}(y)$ of the energy-containing motions would probably be an outcome of a scale interaction, because the wall-normal structure of ν_t in (3) essentially reflects the inhomogeneous turbulent dissipation affected by the multiple scales at different wall-normal locations. In this sense, it would be appropriate to interpret that ν_t in (3) describes a 'minimal' form of scale interaction.

CONCLUSIONS

The inspection of the spectra of the streamwise velocity and the linear theory in § so far has suggested that the near-wall streamwise velocity of the energy-containing motions in the logarithmic and outer regions probably scales in the inner units, while their respective outer part scales in the given length scale of interest. As the inner-scaling nature of a certain flow feature should indicate the viscous wall effect, this observation sounds quite similar to the concept of 'mesolayer' introduced for the mean momentum balance (Long & Chen, 1981; Afzal, 1982, 1984; Sreenivasan & Sahay, 1997; Wei *et al.*, 2005). The linear model analysis indicates that the inner-scale nature of each motion would be intricately linked with the Reynolds-number-dependent behavior of the outer peak location in the streamwise wavenumber spectra of the streamwise velocity (Mathis *et al.*, 2009; Vallikivi *et al.*, 2015) as well as the near-wall penetration of large-scale outer structures. Furthermore, it would lead to 'incomplete' or 'partially broken' self-similarity of the energy-containing motions in the logarithmic region given in the form of Townsend's attached eddies. It should be noted, however, that this is not necessarily inconsistent with the attached eddy hypothesis of Townsend (1976) who used the self-similarity of the energy-containing motions in the logarithmic region as the core of his original theory. In fact, the statistical structure of each attached eddy introduced by Townsend (1976) was built at the 'inviscid' limit by neglecting the viscous effect from the wall. On the other hand, the incomplete self-similarity in the present study appears essentially because the viscous wall effect (i.e. the inner-scaling nature) is incorporated in the structure of the attached eddies. In this respect, the incomplete self-similarity should rather be viewed as a consequence of viscous correction of the original description of Townsend (1976).

Finally, it is worth highlighting that the simple observation made here would enable one to consistently describe several important observations within a single framework: i.e. the viscous effect in the mean momentum balance (Sreenivasan & Sahay, 1997; Wei *et al.*, 2005; Klewicki *et al.*, 2009; Klewicki, 2013), the near-wall penetration of the outer structures via their footprint resulting the inner-outer interaction (Hutchins & Marusic, 2007; Mathis *et al.*, 2009; Agostini & Leschziner, 2014, 2016), and the Reynolds-number-dependent behavior of the outer peak in the streamwise wavenumber spectra of the streamwise velocity (Mathis *et al.*, 2009; Vallikivi *et al.*, 2015), a viscous correction of Townsend's attached eddy hypothesis and the resulting 'incomplete' self-similarity in the region close to the wall (present study), and the collective generation of turbulent skin friction by all the energy-containing motions (Hwang, 2013; de Giovanetti *et al.*, 2016). In this respect, further evidence particularly on other velocity components and Reynolds stress would need to be presented in the future work.

ACKNOWLEDGEMENT

This work was supported by the Engineering and Physical Sciences Research Council (EPSRC) in the UK (EP/N019342/1).

REFERENCES

Afzal, N. 1982 Fully developed turbulent flow in a pipe: an intermediate layer. *Ing.-Arch.* **52**, 355–377.

Afzal, N. 1984 Mesolayer theory for turbulent flows. *AIAA J.* **22**, 437–439.

Agostini, L. & Leschziner, M. 2014 On the influence of outer large-scale structures on near-wall turbulence in channel flow. *Phys. Fluids* **26**, 075107.

Agostini, L. & Leschziner, M. 2016 Predicting the response of small-scale near-wall turbulence to large-scale outer motions. *Phys. Fluids* **28**, 015107.

del Álamo, J. C. & Jiménez, J. 2006 Linear energy amplification in turbulent channels. *J. Fluid Mech.* **559**, 205–213.

Alizard, F. 2015 Linear stability of optimal streaks in the log-layer of turbulent channel flows. *Phys. Fluids* **27**, 105103.

Butler, K. M. & Farrell, B. F. 1993 Optimal perturbations and streak spacing in wall-bounded turbulent shear flow. *Phys. Fluids* **5**, 774–777.

Cess, R. D. 1958 A survey of the literature on heat transfer in turbulent pipe flow. *Westinghouse Research Rep.* pp. no. 8–0529–R24.

Cossu, C., Pujals, G. & Depardon, S. 2009 Optimal transient growth and very large scale structures in turbulent boundary layers. *J. Fluid Mech.* **619**, 79–94.

de Giovanetti, M., Hwang, Y. & Choi, H. 2016 Skin-friction generation by attached eddies in turbulent channel flow. *J. Fluid Mech.* **808**, 511–538.

Hoyas, S. & Jiménez, J. 2006 Scaling of the velocity fluctuations in turbulent channels up to $re_\tau = 2003$. *Phys. Fluids* **18**, 011702.

Hutchins, N. & Marusic, I. 2007 Evidence of very long meandering features in the logarithmic region of turbulent boundary layers. *J. Fluid Mech.* **579**, 1–28.

Hwang, Y. 2013 Near-wall turbulent fluctuations in the absence of wide outer motions. *J. Fluid Mech.* **723**, 264–288.

Hwang, Y. 2015 Statistical structure of self-sustaining attached eddies in turbulent channel flow. *J. Fluid Mech.* **723**, 264–288.

Hwang, Y. & Bengana, Y. 2016 Self-sustaining process of minimal attached eddies in turbulent channel flow. *J. Fluid Mech.* **795**, 708–738.

Hwang, Y. & Cossu, C. 2010*a* Amplification of coherent streaks in the turbulent Couette flow: an input-output analysis at low Reynolds number. *J. Fluid Mech.* **643**, 333–348.

Hwang, Y. & Cossu, C. 2010*b* Linear non-normal energy amplification of harmonic and stochastic forcing in the turbulent channel flow. *J. Fluid Mech.* **664**, 51–73.

Hwang, Y. & Cossu, C. 2010*c* Self-sustained process at large scales in turbulent channel flow. *Phys. Rev. Lett.* **105**, 044505.

Klewicki, J. C. 2013 Self-similar mean dynamics in turbulent wall flows. *J. Fluid Mech.* **718**, 596–621.

Klewicki, J. C., Fife, P. & Wei, T. 2009 On the logarithmic mean profile. *J. Fluid Mech.* **638**, 73–93.

Lee, M. K. & Moser, R. D. 2015 Direct numerical simulation of the turbulent boundary layer over a cube-roughened wall. *J. Fluid Mech.* **774**, p395.

Long, R. R. & Chen, T.-C 1981 Experimental evidence for the existence of the mesolayer in turbulent systems. *J. Fluid Mech.* **105**, 9–59.

Mathis, R., Hutchins, N. & Marusic, I. 2009 Large-scale amplitude modulation of the small-scale structures in turbulent boudnary layers. *J. Fluid. Mech.* **628**, 311–337.

Millikan, C.B. 1938 A critical discussion of turbulent flows in channels and circular tubes. In *Proceedings of the Fifth International Congress of Applied Mechanics*.

Park, J., Hwang, Y. & Cossu, C. 2011 On the stability of large-scale streaks in the turbulent Couette and Poiseulle flows. *C. R. Mècanique* **339** (1), 1–5.

Perry, A. E. & Chong, M. S. 1982 On the mechanism of turbulence. *J. Fluid Mech.* **119**, 173–217.

Pujals, G., García-Villalba, M., Cossu, C. & Depardon, S. 2009 A note on optimal transient growth in turbulent channel flows. *Phys. Fluids* **21**, 015109.

Reynolds, W. C. & Hussain, A. K. M. F. 1972 The mechanics of an organized wave in turbulent shear flow. Part 3. Theoretical models and comparisons with experiments. *J. Fluid Mech.* **54** (02), 263–288.

Schmid, P. J. & Henningson, D. S. 2001 *Stability and Transition in Shear Flows*. New York: Springer.

Schoppa, W. & Hussain, F. 2002 Coherent structure generation in near-wall turbulence. *J. Fluid Mech.* **453**, 57–108.

Sreenivasan, K. R. & Sahay, A. 1997 The persistence of viscous effects in the overlap region and the mean velocity in turbulent pipe and channel flows. In *Self-Sustaining Mechanisms of Wall Turbulence* (ed. R. Panton), pp. 253–272. Comp. Mech. Publ.

Tennekes, H. & Lumley, J. L. 1967 *A first course in turbulence*. MIT Press.

Townsend, A. A. 1976 *The structure of turbulent shear flow*. Cambridge U. Press.

Vallikivi, M., Ganapathisubramani, B. & Smits1, A. J. 2015 Spectral scaling in boundary layers and pipes at very high reynolds numbers. *J. Fluid Mech.* **771**, 303326.

Wei, T., Fife, P., Klewicki, J. C. & Mcmurtry, P. 2005 Properties of the mean momentum balance in turbulent boundary layer, pipe and channel flows. *J. Fluid Mech.* **522**, 303–327.

Weideman, J. A. C. & Reddy, S. C. 2000 A MATLAB Differentiation Matrix Suite. *ACM Trans. Math. Soft.* **26**, 465–519.

Willis, A. P., Hwang, Y. & Cossu, C. 2010 Optimally amplified large-scale streaks and drag reduction in the turbulent pipe flow. *Phys. Rev. E* **82**, 036321.